Requirements for Charged Particle Medical Accelerators -- LBL Experience*

William T. Chu
Lawrence Berkeley Laboratory
University of California, Berkeley, CA 94720

(To be presented at the Workshop on Accelerators for Charged-Particle Beam Therapy, Fermi National Accelerator Laboratory, January 24 and 25, 1985.)

*This work was supported by the US Department of Energy under contract No. DE-AC03-76SF00098 and in part by the National Institute of Health under Grant Ca15184.

I. Introduction

At the Lawrence Berkeley Laboratory of the University of California, Berkeley, the 184-Inch Cyclotron and the Bevalac have provided accelerated heavy ions for biomedical applications ranging from basic research to radiation treatment of human cancer. These experiences coupled with the LBL expertise in accelerator technology have prompted us to plan for a hospital-based heavy-ion medical accelerator (Alpen (1984).

At this proposed facility, accelerated heavy ion beams can be produced suitable for treatment of human cancer. These same beams can be effectively utilized to pursue other clinical and basic research activities. The accelerator system is contemplated to reliably accelerate a wide range of ion species, from helium to argon, to energies as low as 70 MeV/amu for 4-cm range ^{4}He beams to as high as 800 MeV/amu for 30-cm range ^{28}Si beams, with intensities sufficient to limit treatment times to about one minute. Secondary radioactive heavy ion beams, such as ^{11}C and ^{19}Ne, will also be available to aid the accurate treatment planning as well as broaden the base of scientific research that can be conducted at this facility. In addition, the species of ions could be extended to include protons and moderate intensities of ^{56}Fe beams, adequate to support research programs in biophysics and related fields of scientific inquiry.

The beams can be delivered sequentially to multiple treatment rooms to accommodate as many as 100 patients per day in addition to provide for the needs of an intensive program in basic research. Estimates of the projects operating costs for this facility suggest that the incremental cost per patient treatment is modest in the context of alternative radiation treatment. The main accelerator component required to produce 800 MeV/amu beams is a synchrotron ring approximately 30 meters in diameter. Such an accelerator could be located in a major medical complex to provide cost-effective medical care and to support a forefront research program in high technology medicine.

II. Advantages of High-LET Charged Particle Beams

There is a strong rationale to perform a randomized radiotherapy trial with heavy charged particles at a hospital-based facility. The hypothesis to be tested may be briefly formulated as follows: Given the fact that particle beams of both low and high atomic numbers can achieve superior dose localization, will the heavier ions produce better local control of human cancer than light ions? We expect better results because of the advantageous radiobiological characteristics of the heavier ions.

Hypoxic parts of tumer tissues, for example cells located near necrotic foci, are much more resistant to conventional radiation. Experiments have shown, however, that while this resistance exists for low-LET charged particle irradiation, it does not exist for heavy-ion irradiation: Hypoxic cells are nearly as sensitive to heavy-ion irradiation as oxic cells.

Cells in rapidly growing tumers are asynchronous. Cells in the S phase of the DNA synthesis cycle are much more resistant to low-LET radiation than cells in other phases of the cycle; therefore, in protracted radiotherapy there are usually surviving cells that are protected against low-LET radiation. Heavier charged particles such as Si ar Ar ions greatly diminish the differences in radiosensitivity for cells at any phase of cell division; fewer protected cells are expected to survive after a dose of heavy ions.

There are several types of molecular repair mechanisms known in cells exposed to low atomic-number particles at low LET. Such repair becomes largely ineffective when heavy ions are used. As a result the Bragg peaks of heavy ions are much effective than low-LET radiations.

The combination of these factors is expected to make heavy ions particularly effective for the treatment of well-localizable tumors that have radioresistant cell populations.

In addition, maximizing the dose to the local cancer while minimizing dose to the surrounding normal tissues offers the highest potential for tumor control. The physical properties of charged particles, including heavy particles and protons, permit dose localization superior to that achievable with neutrons. The particle range, or degree of dose localization in the patient, can be determined with great precision by technique which utilize radioactive beams, such as ^{11}C and ^{19}Ne, and positron emission tomography. Superior treatment planning and verification can be achieved with these particle compared with any other radiation modality including protons and helium nuclei.

Fig. 1 demonstrates how the consideration of both physical dose localization advantage and the corresponding enhancement of biological cell killing effectiveness influences the various radiation modalities. the abscissa in these plots is the ratio of biologically effective doses defined as:

$$\text{Effective dose ratio} = \frac{(\text{Dose} \times \text{RBE}_{50}) \text{ at mid target volume}}{(\text{Dose} \times \text{RBE}_{50}) \text{ at entrance}}$$

It is regarded as more advantageous to use the charged particles that are further out to the right on this axis of the effective dose ratio. When the effective dose ratios are comparable, the modalities that exhibit lower OER (Oxygen Enhancement Ratio) will be the better choice.

The data are based on measurements made with the cultured cells <u>in vitro</u>. The top panel is constructed for a 10-cm x 10-cm x 4-cm deep field with the distal edge of the target volume at 14-cm deep. The bottom panel is for a 10 x 10 x 10 cm^3 target volume with the 24-cm deep distal edge.

For smaller, more shallow target volume (top panel), it appears that C, Ne, and negative pion beams are superior in their ratio of bilogically effective doses. Ar and Si ion beams and p and He ion beams are intermediate in this ratio, but quite different from each other with respect to their OER values.

For a larger, deeper tumer volume (bottom panel), the C and He ion beams are quite similar, as are the Ne ion and negative pion beams; however, there are quite distinct division on OER values between low-LET and high-LET particle beams.

III. Dose Localization

The localization of the radiation dose in the target volume is limited by many causes. The range straggling of the charged particles in the slowing medium makes the distal edge of the radiation field not sharp. The energy spread in the accelerated beams, as well as the energy fluctuation from pulse

to pulse result in the same effect. The emittance of the beam and the multiple scattering of the charged particles in the beam path and inside the patient body both contribute in the lateral spreading of the beam and broader penumbra. Also these effects lower the peak-to-plateau ratios of the charged particle beams that are collimated to small sizes.

(A) Energy Loss Rate for Heavy Charged Particles:

A heavy projectile, much more massive than an electron, of charge Ze, incident at speed βc (β>>1/137) through a slowing medium, dissipates energy mainly bia interactions with the electrons of the medium. The mean rate of such energy loss per unit length x, dE/dx, called the stopping power, is given by the Bethe-Bloch equation. The stopping power is closely related to LET (Linear Energy Transfer). The LET is proportional to the square of the charge of the incident particle, to the reciprocal of kinetic energy (1/E), and to the electron density of the slowing medium.

We may approximately treat media which are chemical mixtures or compounds by computing (Bethe and Ashkin (1959))

$$\frac{dE}{dx} = \Sigma \left(\frac{dE}{dx} \right)_i$$

with (dE/dx) appropriate to the i-th chemical constituent, using the partial density in the formula for dE/dx. For many chemical compounds, small corrections to this additivity rule may be found in Berger and Seltzer (1982).

In the stopping region, the stopping power formula becomes inapplicable. At the very slowest speeds, total energy loss rates are proportional to β. The energy loss rate passes through a small peak at intermediate speeds due to elastic Coulomb collisions with the nuclei of the slowing medium (Sidenius (1974)) and rise through a larger peak at projectile speeds comparable to atomic speeds (β on the order of αc).

The mean range, R, of the charged particles in the slowing medium is obtained by integrating the stopping power equation given above:

$$R = \int_E^0 \frac{dE'}{dE'/dx}$$

The range-energy relationship for several heavy ions in water were calculated by Stewart (1967). Measurements and calculations of range-energy relationship for heavy ions were also made by Northcliffe (1963), by Barkas and Berger (1964), and by Eby and Morgan (1972). For a given medium, the range R' of any other beam particle with mass M' and charge Z' is given in terms of the range R of other particle with mass M and charge Z and having the equal velocity is given by

$$R' = \frac{M'/M}{Z'/Z} R$$

(B) Straggling:

Straggling is a dispersion in path length distribution as a result of statistical fluctuations in the energy loss processes. it was shown by Lewis (1952) and by Berger and Seltzer (1964) that the distribution is Gaussian. However, we know that there are small deviation from this distribution.

For a particle of initial energy E and mean range R, proceeding in the direction x, the range distribution may be written in the form:

$$s(x) = \frac{1}{\sqrt{2\pi}\,\sigma_x} \exp\left(-\frac{(x-R)^2}{2\sigma_x^2}\right)$$

where σ_x is the variance in the path length distribution for particles of range R. There are special corrections to this formula at high and low kinetic energies.

since the atomic composition of soft tissues is similar to that of water, we may use an approximate practical expression for water:

$$\sigma_x \text{ (water)} = 0.0120 \frac{R^{0.951}}{\sqrt{A}}$$

In the range of validity of this formula ($2 < R < 40$ cm), σ_x is almost proportional to range, R, and is inversely proportional to the square root of the particle mass number, A. The relationship between the range and the straggling for various ion beams are shown in Fig. 2(b).

For the range of 20-cm in water, σ_x for various ions are:

Ions	σ_x
Neon	0.046 cm
Carbon	0.06
Helium	0.1
Proton	0.2

The straggling for 20-cm range protons is 4.5 times greater than that for the same range neon nuclei.

(C) Multiple Scattering:

The particles of the beam are deflected in collisions with nuclei of the slowing material. Many of these collisions result in small angle deflections, and multiple scattering leads to a divergence of the beam and to a radial spreading of the particle away from ideal straight line tranjectories. The bulk of deflections is due to elastic Coulomb scattering.

There is a small correction due to the contribution of strong interactions to the total multiple scattering for the hadronic projectiles. The angular distribution from the multiple scattering is roughly Gaussian only for small deflection angles, while it shows much greater probability for large-angle scattering than the Gaussian would suggest.

At range R the projected radial distribution of deflection y of the particle is given by:

$$P(y) = \frac{1}{\sqrt{2\pi}\,\sigma_y} \exp\left(-\frac{Y}{2\sigma_y^2}\right)$$

where σ_y is approximately given by:

$$\sigma_y = \frac{0.0294\ R^{0.896}}{Z^{0.207}\ A^{0.396}}$$

The relationship between the ranges and the multiple scattering for various ion beams are shown in Fib. 2(c). For the range of 20-cm in water, σ_y for various ions are:

Ions	σ_y
Neon	0.082 cm
Carbon	0.11
Helium	0.22
Proton	0.43

The multiple scattering for protons is about 5 times greater than that for the same range neons.

(D) Emittance of the Beam

The emittance of the extracted beam determines the phase space of the charged particles tranported into the target volume. For example, if we consider the Ne ion beam of 20-cm range R with a diameter D of 5-cm (e.g., beam spot size for scanned beam), the multiple scattering gives $\sigma_y \approx 0.05$ cm. A comparable divergence is attained if the emittance is $\epsilon \approx D\,\sigma_y/R \approx 1 \times 10^{-4}$ meter-radian. For focal lesion application, we take 10-cm range of C ion beam with a diameter of 0.5 cm, then the multiple scattering gives $\sigma_y \approx$ 0.1 cm. The comparable divergence is obtained for the emittance $\epsilon \approx 4 \times 10^{-5}$ m-rad.

The design value of the emittance for the proposed accelerator is 2×10^{-5} m-rad, which is about a half of the above estimates. Since the effects of the multiple scattering and emittance add statistically, 1/2 as big divergence due to the finite size of emittance contributes only 1/4 in the spreading of penumbra.

(E) Peak-to-Plateau Ratios and Penumbra

The diverging beams and multiple scattering in the slowing medium generally broaden the beams, and lower the peak-to-plateau ratios. The effect is more pronounced for smaller beams as more particles scatter out of the original trajectories than those scattering in. Fig. 3 shows the 20-cm range proton and He ion beams: the central-ray doses for large beams and collimated beams are normalized at the entrance. Experimentally measured Bragg curves for 225 MeV/amu He ion beam and for 308 MeV/amu C ion beam are shown in Fig. 4 as a function of residual ranges.

The dose profiles of proton and C ion beams through a 1-cm slit are depicted in Fig. 5. The proton beam profiles are shown either normalized at the peak or at the entrance. The former shows that the penumbra for proton beam is about square-root of 12 times bigger than that of C ion beam, and the latter shows that the peak-to-plateau ratio is decreased by about 40% for proton beam compared with that of C ion beam.

Our experiences in clinical situations using He ion beams at the 184-Inch Cyclotron and the heavy ion beams at the Bevalac generally support the above analyses. The double scattering system that laterally spreads the beam by scattering materials in the beam path also contributes in broadening the penumbras. The wobbler system, that uses no scattering material in the beam path, produces narrower penumbra compared with those obtained through the double scattering method.

(F) Radioactive Beam Ranging Technique

Although the charged particle beams exhibit sharply defined ranges as discussed above, the accuracy of delivering the radiation dose into a well-defined target volume is only as accurate as the knowledge of the integral water-equivalent thickness of the intervening tissues. The x-CT supplies information on the distribution of x-ray absorption coefficients, and accurate conversions of the x-CT data into the stopping powers of the medium for charged particles are not possible. The He and Ne ion measurements using a frozen beagle and comparing them with x-CT data indicates that the x-CT measurements are off as much as 0.4 cm out of 5 cm range in brain and thorax (Table 2). The MRI data may augment the x-CT data by measuring the chemical composition of the tissues, yet they are not sufficient to supply the information of the stopping power of the tissues. Whereas the stopping radioactive beams directly measure the integral stopping power of the medium in water equivalent thickness.

Positron emitters, C^{11}, N^{13}, O^{15}, F^{17}, and Ne^{19}, result when their respective stable parent particles, C^{12}, N^{14}, O^{15}, F^{18}, Ne^{20}, pass through an absorbing material. For example, 530 MeV/amu Ne^{20}, beam is put through a 2.5-cm thick Be slab, and momentum analyzing the resulting beam separates the radioactive Ne^{19} beam from the Ne^{20} beam. The added energy spread of the radioactive beam mainly comes from the Fermi momentum of the nucleons in the target nuclei which collide with the incident parent nuclei. A negligible contribution is from the slight difference in dE/dx for Ne^{19} and Ne^{20}

particles, and the fact that the Ne^{19} productions take place distributed across the entire target thickness. The experimentally measured Bragg curves for Ne^{20} and Ne^{19} beams are shown in Fig. 6(a & b). As schematically shown in Fig. 6(c), the range of the radioactive beam is modulated and it is brought to a stop in a precisely defined position in the patient (e.g., the distal egdge of the target volume) by determining the stopping region using a positron emission tomographic camera. The integral water-equivalent thickness of the intervening tissues is simply given by the range of the incident radioactive beam. In this process, the water-equivalent thickness measured using one kind of radioactive beam, e.g., Ne^{19}, is the property of the slowing medium and indepedent of the species of ions used. And therefore it may be applied for therapy planning using any kind of charged particle beams. We have already used the Ne^{19} ranging techniques in several human patients treated with heavy ion beams.

Another application of radioactive beams that appears to have promise is that of injecting a bolus of a particular positron metabolic or flow rates by measuring positron emitter activity as a function of position and time after the beam injection. The absence of radioactivity at location other than those being studied would make for a very clean technique, provided that the hot atom chemistry of the injected ions is well understood.

IV. Requirements for Heavy Ion Medical Accelerator

The requirements for heavy ion medical accelerator are different for different applications of the machine. The applications may be broadly divided into five different uses: namely, radiation treatment of cancer, focal lesion, radioactive beam ranging, radiation biology, and physics. In Table 3, the requirements for these users are listed; the requirements for radiation biology are not listed separately, since its needs are quite similar to those of therapy, focal lesion, and radioactive beams. In Table 3, when applicable, the optimal requirement is listed above the minimal requirement for each category.

The ion species requested ranges from He to Si or Ar. There are interests in obtaining higher Z particles, such as Fe, La, Au, and even U. The ranges of these particles requested for clinical uses span from the 4-cm range He ions to the 30-cm range Si ions. To obtain 37-cm Ne^{19} beam, the radioactive beam users like to have 40-cm Ne^{20} beams. Range-energy relations for various ions are shown in Fig. 7. From these curves, it is seen that an energy of approximately 800 MeV/amu is required to provide a 30-cm range in tissue for Si ions. For particles lighter than Si, such as C and Ne ions, the 800 MeV/amu capability provides a range in tissue considerably greater than 30 cm.

For tumor sizes and treatment plans typically encountered in the ongoing heavy-ion radiotherapy program at the Bevalac, the minimum on-target intensity requirement of 3×10^7 Si ions per second corresponds to approximately 100 rad per minute. The radioactive beam users places the highest particle flux requirement, 10^{11} particles per second for C and Ne ions, as they depend on

the secondary particles whose intensities are only a fraction of the primary particles (e.g., 10^{-3} for Ne^{19} obtained from 530 MeV/amu Ne^{20} through 2.5-cm Be target).

The upper limits for the energy spread (dE/E) of the accelerated beams and the pulse-to-pulse energy fluctuations are placed at 0.1% FWHM. The most strigent requirement of particle beam emittance is placed by the focal lesion applications which use very tightly collimated small beams. Their request is that the emittance be smaller than 2×10^{-5} meter-radian. The duty factor of 75% is generally requested, since most of the clinical applications avoid unnecessarily high instantaneous dose rates. This requirement becomes more important for dynamic beam delivery systems, in which the complexities of the beam handling increase inversely to the length of available time in which to accomplish the task.

It is also desirable for the dynamic modes of beam delivery to extract the accelerated particles with the following characteristics. The intensities of the extracted beam should be uniform over the time, since the wobbling or scanning systems translate the time-structure of the beam into spatial fluctuations. The extraction level and duration of the spill should be reliably controllable. The beam optics for extracted beams must remain stable for a wide range of extraction levels (up to 3 orders of magnitude) and spill lengths.

In general, most of the clinical applications call for long spills; there are occasions that use very short beam pulses. In imaging moving organs in the patients, one would like to have a spill of 1 millisecond duration. Also in studying the high dose-rate biology and physics, very high instantaneous dose rate of short durations is required.

From the practical point of view of using the accelerated heavy ion beams for human patients, all users request short planned delays and down times and few unplanned interruptions. When two different ions are used, the time to switch the ion species is to be 20 seconds, or not more than 2 minutes at most. Similar requests are put on the energy change of a given ion beam. Such a capability will eliminate the need of mechanical beam energy degrader which produces unwanted fragments and lower the beam quality. For dynamic mode of beam delivery, the change of energy in small steps from a pulse to the next pulse will be useful.

In multi-room operation using a single accelerator, several patients will be readied for irradiation at the same time, and some waiting for the patients will be unavoidable. Allowable wait is 5 minutes. Fast beam switching and short treatment time are important; but clearly logistics and planning of patient flow are the deciding factors.

The accelerator specifications that satisfies these requirements are summarized in Table 4. These machine characteristics have been determined from the experience of ongoing LBL programs and from studies over the past ten years, including the LBL/Arizona Design Study (LBL-7230) completed in 1977.

V. Conclusion

Our general goals are to produce precisely located and sharply defined heavy-ion induced radiolesions in target volume. Heavy ion beams aided with the radioactive beam ranging technique attain these goals much better than the proton beams. In addition we wish to deliver to accurately defined tumor regions high doses of heavy charged particle beams at the highest atainable LET while minimizing radiation effects to surrounding normal tissues. The high LET field will minimize the radiobiological oxygen effect, it will reduce radiobiological repair and differences in radiosensitivity during the cell cycle. It will delay cell progression and reduce sensitivity differences between normal and tumor cell populations.

We believe that the proposed heavy-ion medical accelerator could be built in a major medical complex to provide cost-effective medical care and to support a forefront research program in high technology medicine and basic sciences.

Acknowledgement

The author would like to acknowledge the stimulating discussion with Professor C. A. Tobias, Dr. Eleanor Blakely for data on biological comparison of charged particles, Dr. Aloke Chatterjee for data on radioactive beam, and Dr. Sandra Zink for clinical data.

References

Alonso, J.R., Chatterjee, A. and Tobias, C.A. (1977). High purity radioactive beams at the Bevalac. IEEE Trans. Nucl. Sci., NS-26, 3003-3005.

Alpen, E.L. (1984). The Heavy Ion Medical Accelerator Final Design Summary, Lawrence Berkeley Laboratory, University of California, PUB-5122.

Barkas, W.H. and Berger, M.J. (1964). Studies in penetration of charged particles in matter. NAS-NRC 1133.

Berger, M.J. and Seltzer, S.M. (1982). Mean excitation energies for use in Bethe's stopping-power formula, p. 57-74, Proceedings of Hawaii Conference on Charge States and Dynamic Screening of Swift Ions.

Bethe, M.J. and Ashkin, J. (1959). Experimental Nuclear Physics, Vol. 1, E. Segre, editor, John Wiley, New York.

Eby, P.B. and Morgan S.H. (1972). Phy. Rev. A5, 2536.

LBL-7230 (1977). Dedicated Medical Ion Accelerator Design Study, Final Report, Lawrence Berkeley Laboratory, University of California, Report LBL-7230.

Lewis, H.W. (1952). Phys. Rev. 85, 20.

Northcliffe, L.C. (1963). Passage of heavy ions through matter. Am. Rev. Nucl. Sci. 13, 67.

sidenius, G. (1974). Det Kong. Danske Viden. Selskab Mat. - Fysk. Med. 39, No. 4.

Stewart, P.G. (1967). Calculation of Stopping Power. Lawrence Berkeley Laboratory Report UCRL-17314.

Figure Captions:

Fig. 1 Ratio of biologically effective doses vs. OER for various radiation treatment modalities. The upper panel represents a 10 cm x 10 cm field at 10-14 cm tissue depth. The lower panel represents a 10 cm x 10 cm field at 14-24 cm tissue depth. Available cell data in vitro were used for the construction of this plot.

Fig. 2 Multiple scattering and straggling characteristics for various charged particles as a function of the range.

Fig. 3 Calculated Bragg curves on the central rays of large and small fields of proton and He ion beams.

Fig. 4 Measured Bragg curves of He and C ion beam with same residual ranges.

Fig. 5 Beam profiles of proton and C ion beams through 1-cm slit.

Fig. 6 (a) Bragg curve for 530 MeV/amu Ne-20 beam in water.
(b) Bragg curve of Ne-19 beam obtained from the Ne-20 beam of (a) by letting the parent particles traverse a 2.5-cm Be slab and momentum analyzing the resulting beam.
(c) Schematic diagram of setup for end-of-range localization of a radioactive beam.

Fig. 7 Range-energy curves showing the depth to which various ions will penetrate in tissue.

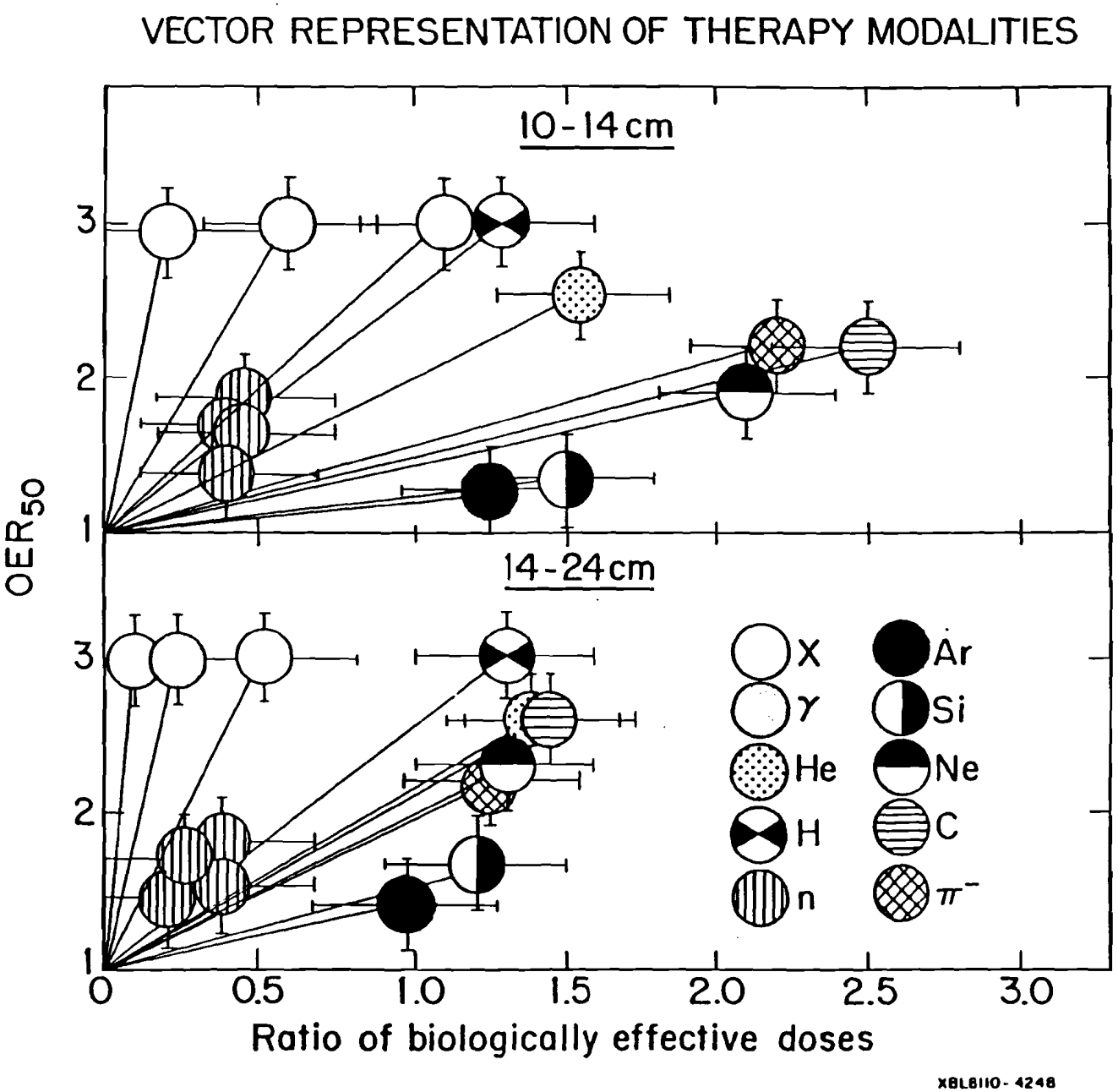
VECTOR REPRESENTATION OF THERAPY MODALITIES
10-14 cm
14-24 cm
OER50
3
2
1
0
0.5
1.0
1.5
2.0
2.5
3.0
Ratio of biologically effective doses
X
γ
He
H
n
Ar
Si
Ne
C
π⁻
XBL8110-4248

FIG. 1

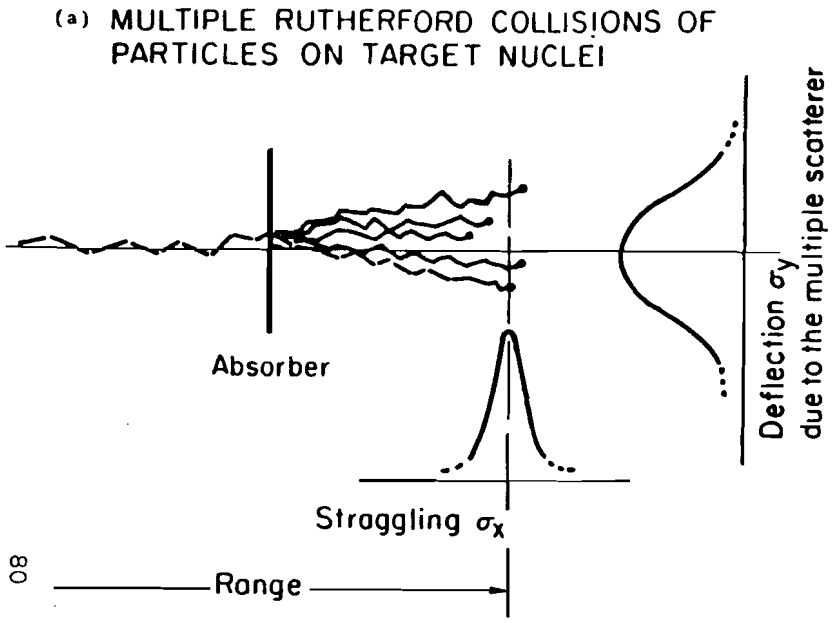

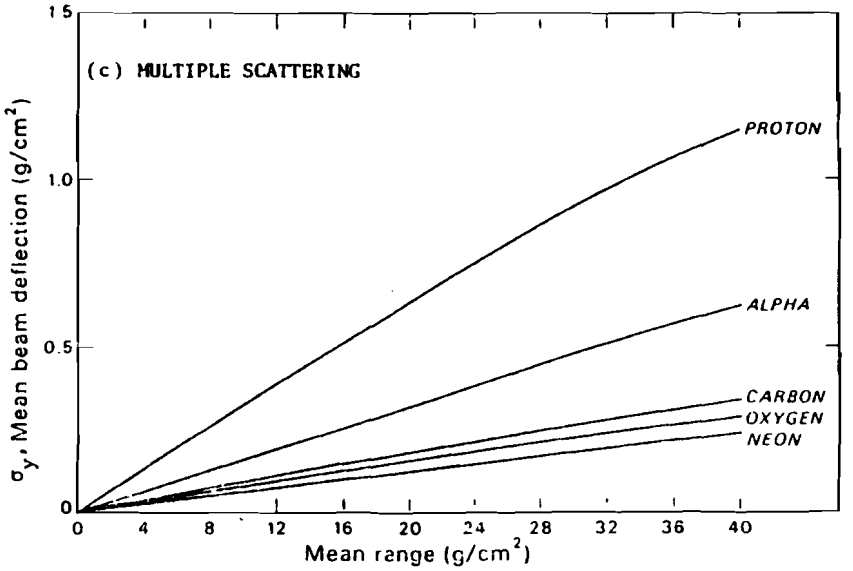

$$\sigma_x \, , \sigma_y \propto \frac{1}{\sqrt{M_{particle}}}$$

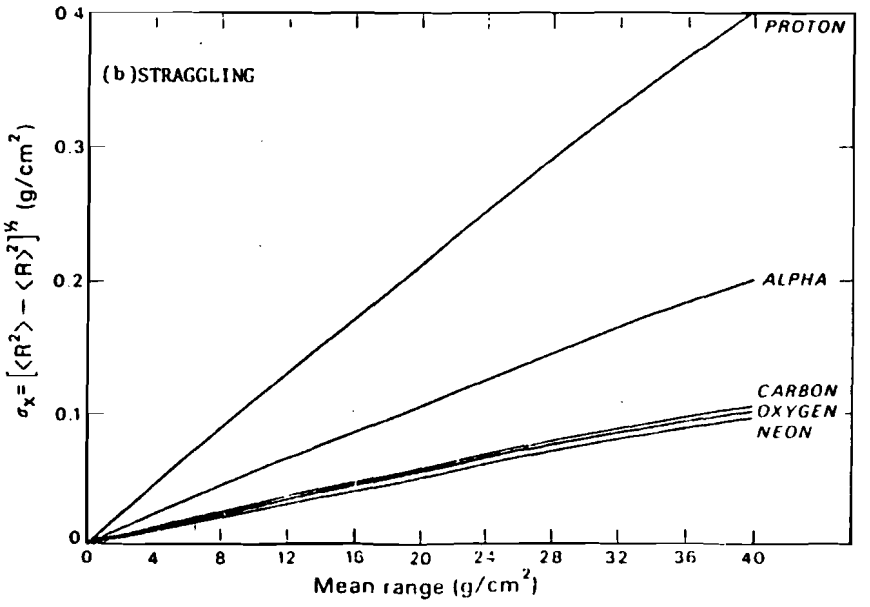

XBL811-3516

FIG. 2

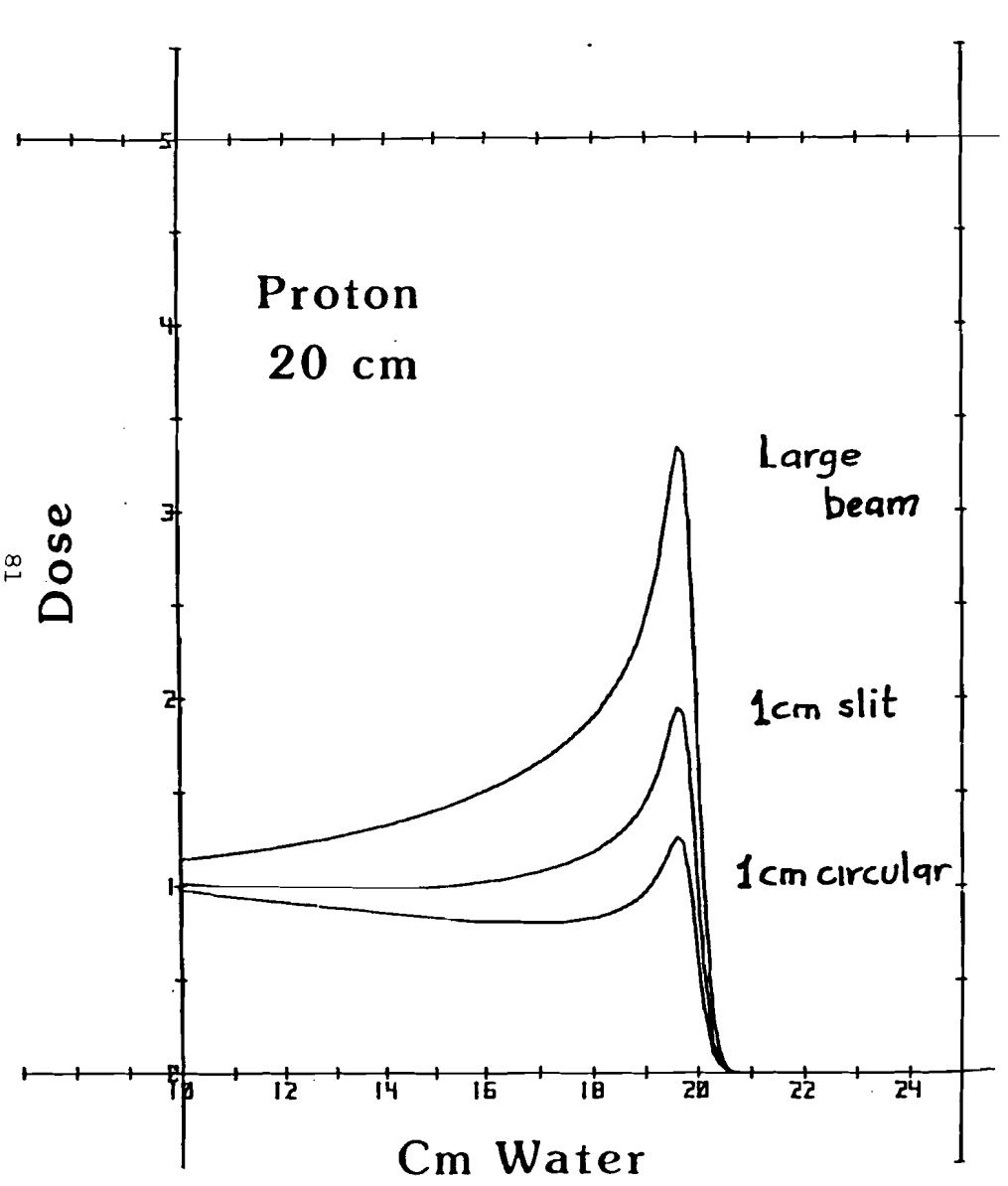
Proton
20 cm
Large beam
1cm slit
1cm circular
Dose
Cm Water
10
12
14
16
18
20
22
24

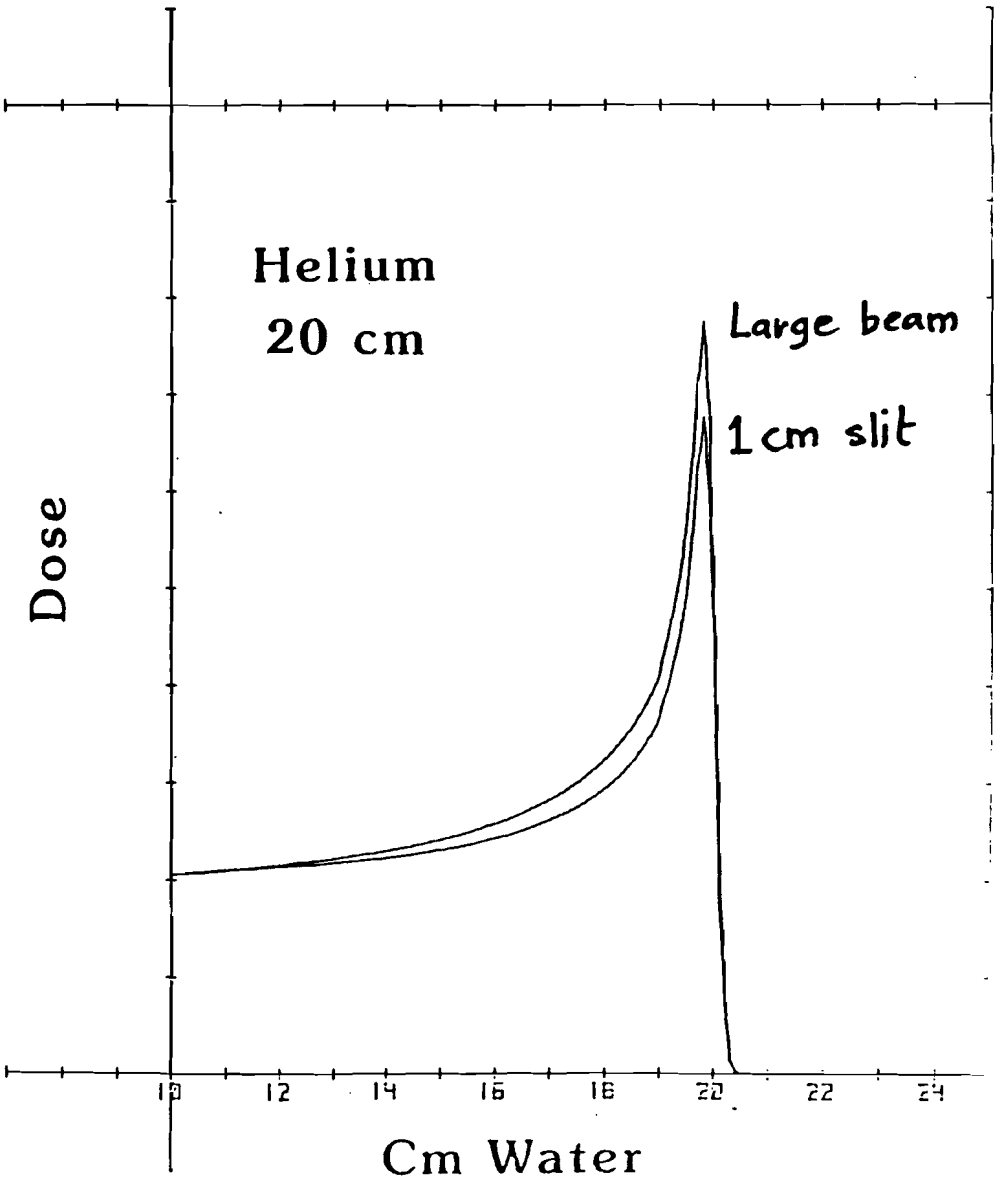
Helium
20 cm
Large beam
1cm slit
Dose
Cm Water
10
12
14
16
18
20
22
24

FIG. 3

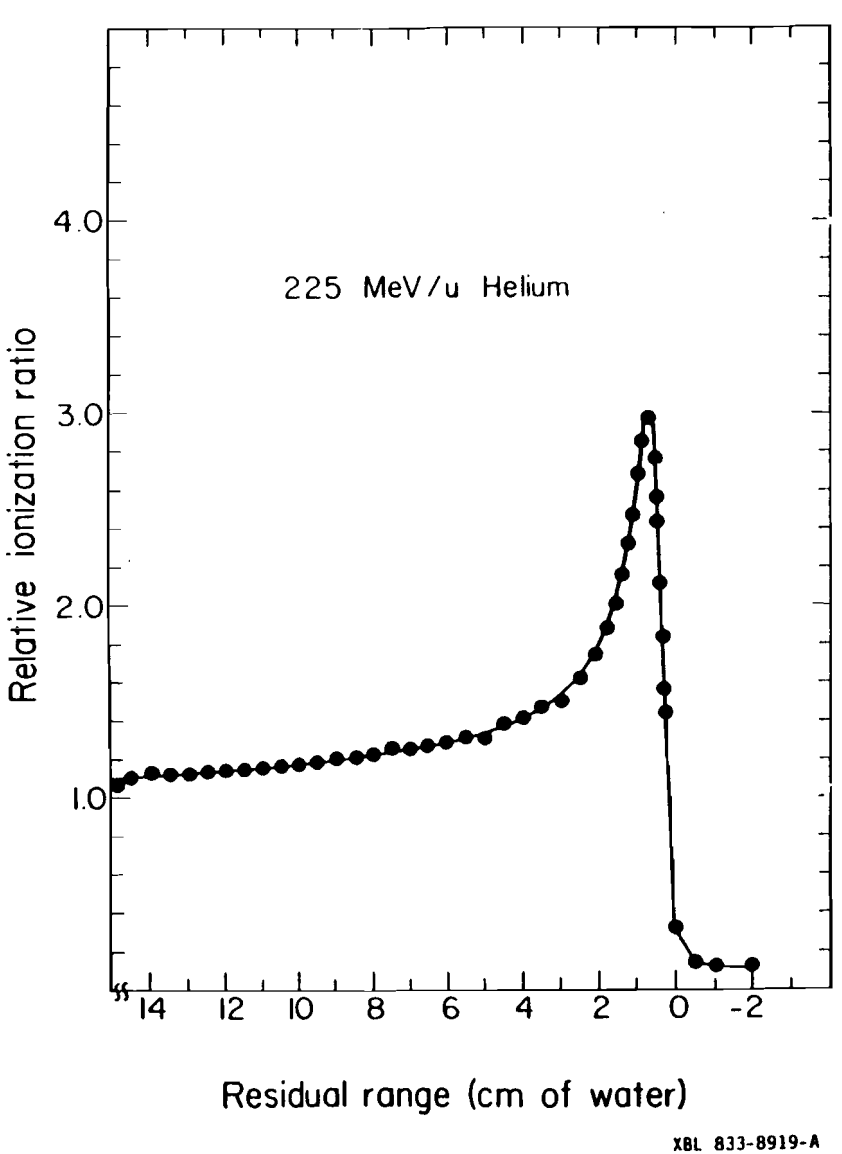
225 MeV/u Helium
Relative ionization ratio
4.0
3.0
2.0
1.0
14
12
10
8
6
4
2
0
-2
Residual range (cm of water)
XBL 833-8919-A

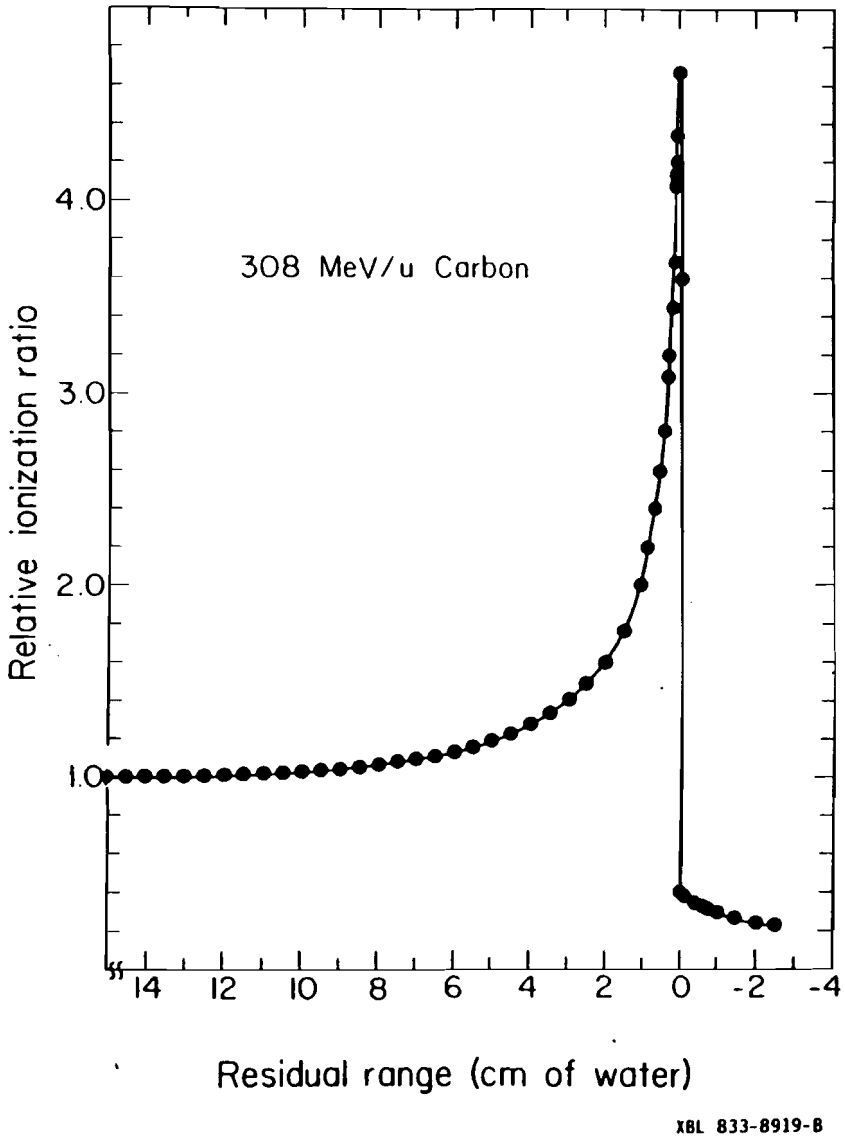
308 MeV/u Carbon
Relative ionization ratio
4.0
3.0
2.0
1.0
14
12
10
8
6
4
2
0
-2
-4
Residual range (cm of water)
XBL 833-8919-B

FIG. 4

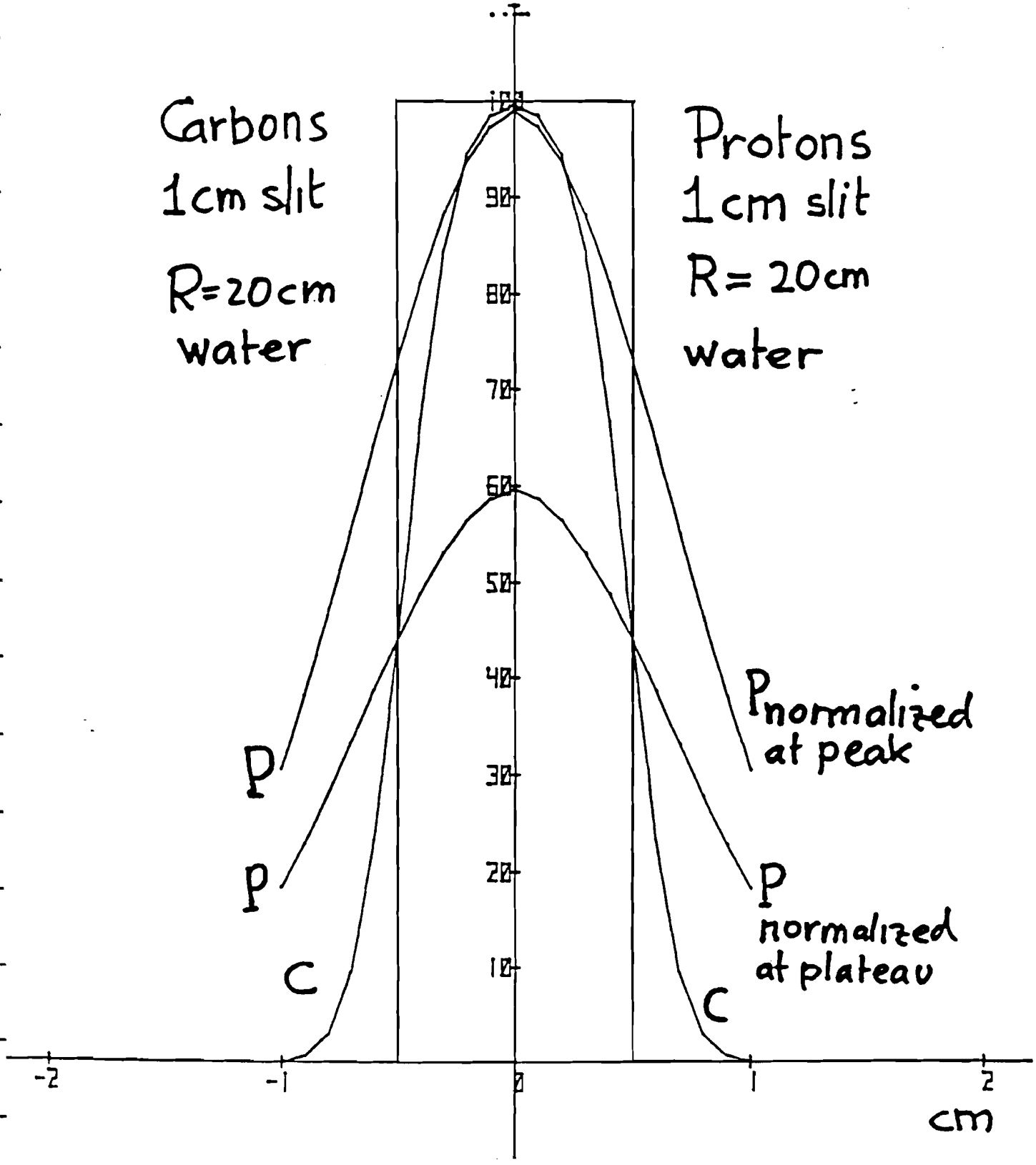
Carbons
1cm slit
R=20cm
water
Protons
1cm slit
R= 20cm
water
100
90
80
70
60
50
40
30
20
10
0
P
P
C
Pnormalized
at peak
P
normalized
at plateau
C
-2
-1
0
1
2
cm

FIG. 5

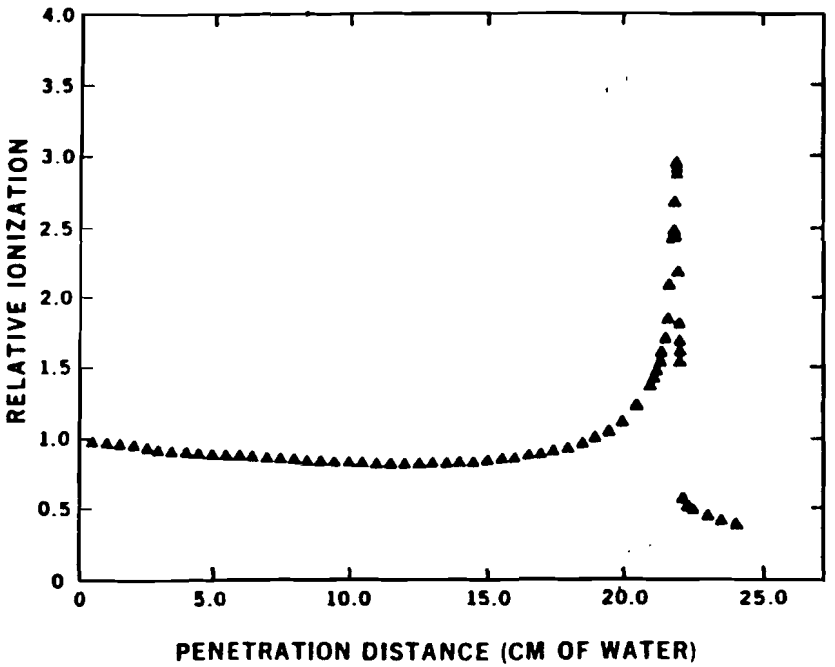

(a) Bragg curve (rate of energy loss per unit path length) for a Ne-20 beam in water.

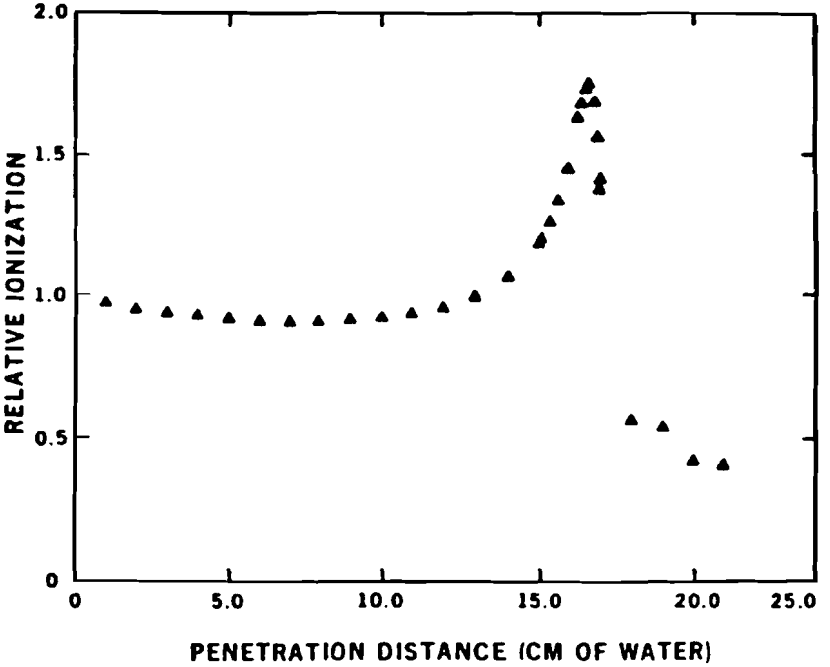

(b) Bragg curve for a Ne-19 beam obtained from the Ne-20 beam of (a) by letting the parent beam traverse a Be block and momentum analyzing the resulting fragments before delivery to a treatment room.

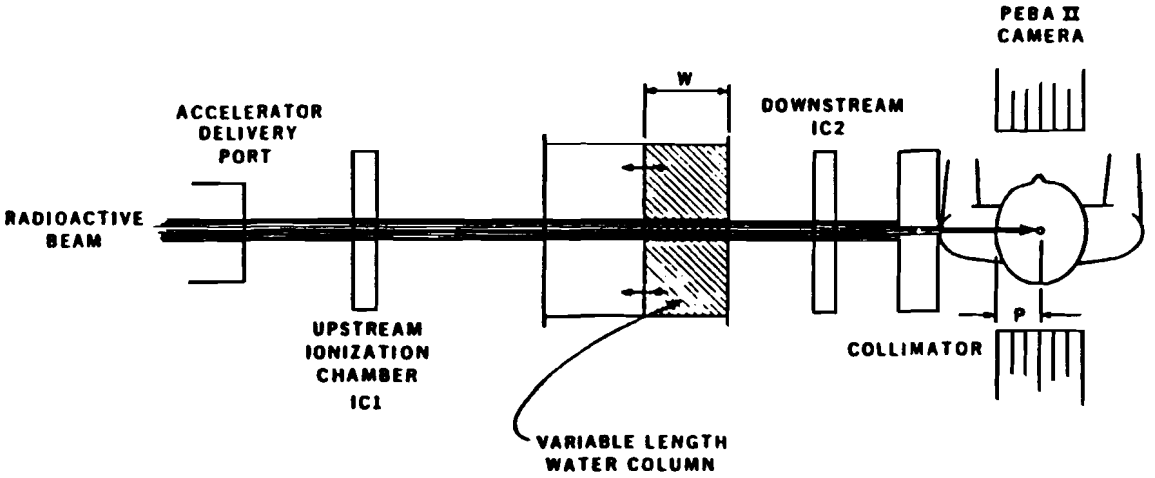

(c) Schematic diagram of a setup in a BEVALAC treatment room for end-of-range localization of a radioactive beam.

FIG. 6

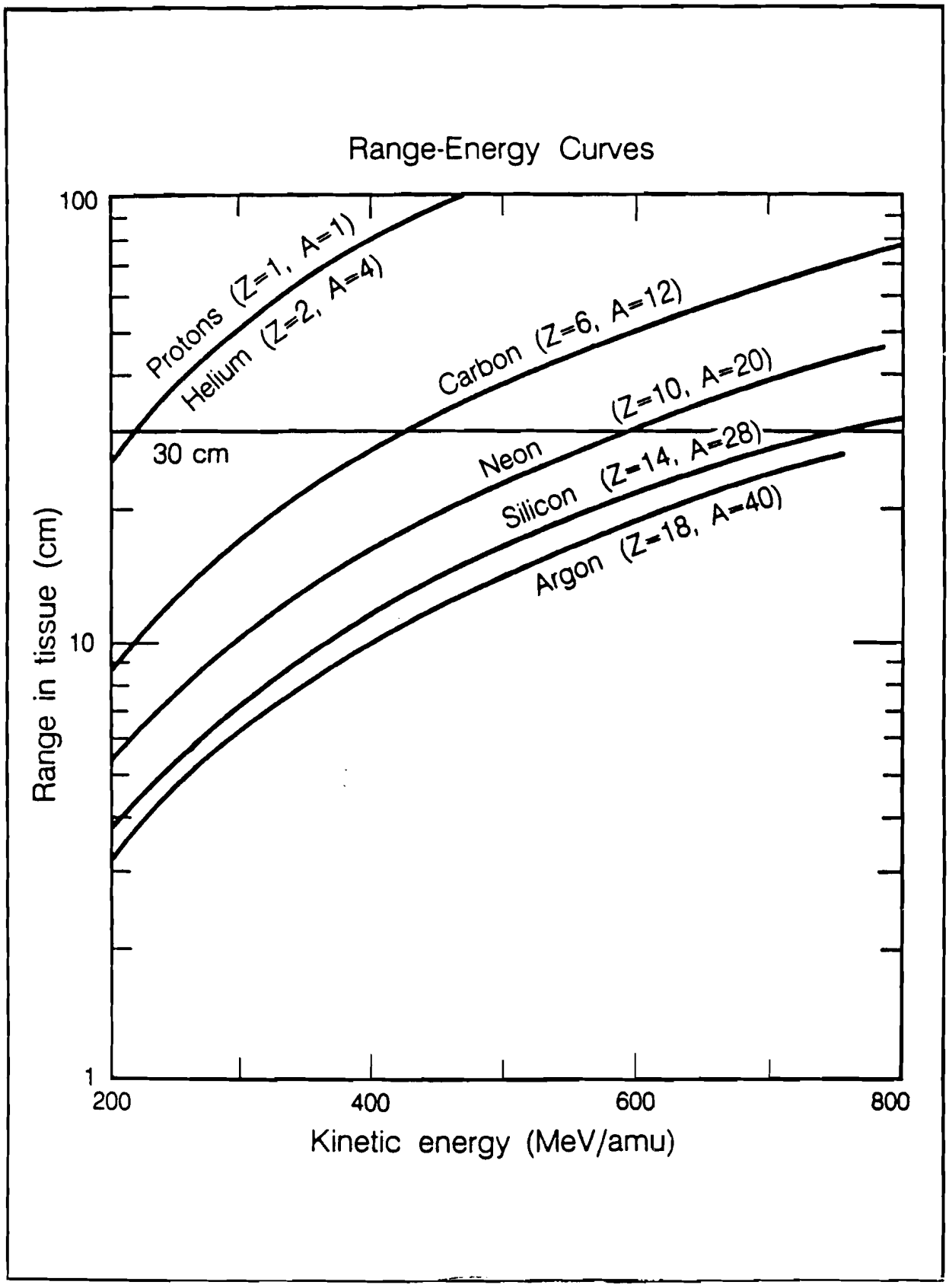

Fig. 7. Energy-range curves showing the depth to which various ions will penetrate in tissue.

Monoenergetic Particle Beams

at the Bevalac

Range 20 cm	Proton	Helium	Carbon
Large beam			
Peak to Plateau	2.9	3.9	3.8
Fragments	0.07	0.15	0.6
Scatter deflection cm	0.75	0.4	0.25
Straggling of range cm	0.8	0.4	0.27
Beam 1.0 cm wide peak to plateau	0.8	1.9	2.7
RBE peak to plateau	1.2	1.6	2.6
Merit factor	1	3	7

19B RABID6.LIN: CAT July 84

TABLE 1. PHYSICAL CHARACTERISTICS OF PROTON, HE AND C ION BEAMS

TABLE 2.

Water Equivalent Thickness (cm) Using a Frozen Beagle

Location	Neon	Helium	CT Scanner
Brain	4.90 ± 0.10	4.85 ± 0.10	5.25 ± 0.10
Back	6.60 ± 0.10	6.68 ± 0.10	6.7 ± 0.15
Thorax (beam from left side)	no data yet	6.80 ± 0.10	7.0 ± 0.2
Thorax (beam from right side)	no data yet	4.60 ± 0.10	5.0 ± 0.2
Upper Abd.	7.65 ± 0.10	7.65 ± 0.10	7.8 ± 0.2
Lower Abd.	7.90 ± 0.10	7.85 ± 0.10	7.85 ± 0.1

TABLE 3.

MEDICAL ACCELERATOR REQUIREMENTS — Optimal/Minimal requirements

	Therapy	Focal lesion	Radioactive Beam	Radiological physics experiments
	- - - Radiation Biology - - -			
Ion species	He -- Si, Ar	He - Si C - Ne	C, Ne	C - Ne , Fe, La, to U C
Range (cm)	4 - 32 6 - 28	4 - 22 6 - 17	6 - 40 8 - 32	10 cm for breast 37 cm for body
Energy spread $\Delta E/E$ (% FWHM)	0.1 0.2	0.1 0.2	0.1 0.3	0.1
Pulse to pulse energy variation $\Delta E/E$ (% FWHM)	0.1 0.2	0.1 0.2	0.1 0.3	0.1 0.5
Intensity at target	600 rad-l/min	10^4 - 10^{10} / pulse 10^4 - 10^8 / pulse	10^6 - 10^7 /pulse 10^5 - 10^6 /pulse Secondary particles	10^3 - 10^5 /cm^2 pulse
Extracted flux (particles/sec)	He $2 \times 10^{10}_{9}$ C $4 \times 10_{9}$ Ne 2×10^{9}		C^{12}_{20} 10^{11}_{11} Ne 10^{11}	
Repetition rate (Hz)	1 1/3	2 1/3	5 1/3	>1
Duty factor (%)	75 25	75 25	25 10	50 25
Emittance (m-rad)	10^{-4}	2×10^{-5} 6×10^{-5}	10^{-4}	$< 6 \times 10^{-4}$
Short pulse duration (msec)		>50		<1 50
Time required to switch ion species (sec)	20 120	20 120	20 120	20 120
Time required to change energies (sec)	20 120	20 120	20 120	20 120
Reliability (% machine up time)	99 95	99 95	99 95	99 95
Waiting time behind other users (minutes)	5	5	10	5

Table 4

Accelerator Requirements

Particle Species:	^{1}H or $^{4}He \rightarrow {}^{28}Si$, ^{40}Ar
Maximum energy:	30-cm-range ^{28}Si (800 MeV/amu)
Minimum energy:	4-cm-range ^{4}He (70 MeV/amu)
Intensity:	$\geqslant 3 \times 10^{7}$ Si ions/sec on target
Duty factor	20−50%
Reliability:	> 95%
Repetition Rate:	0.25 − 4 Hz
Emittance:	$< 2 \times 10^{-5}$ m-radians
Momentum spread	$\Delta p/p$: $1-2 \times 10^{-3}$